

Observation of Shrinkage during Evaporative Drying of Water-Based Paper Coatings

Giuliano M. Laudone,[†] G. Peter Matthews,^{*,†} and Patrick A. C. Gane[‡]

Environmental and Fluid Modeling Group, University of Plymouth, Plymouth PL4 8AA, U.K., and Omya AG, CH-4665 Oftringen, Switzerland

Coated paper for high-quality printing comprises a fine particulate mineral coating, applied as an aqueous suspension and fixed to the fibrous paper substrate with a binder. The shrinkage occurring while the coating layer dries onto the substrate has been measured by observing the deflection of strips of a synthetic substrate coated with ground calcium carbonate with different binders. The force acting on the surface of the strips to cause a given deflection has been calculated using the elementary beam theory. The porosities of the dry structures were measured by compression-corrected mercury porosimetry. We show that the shrinkage occurring during the drying of the coating layer is mainly due to capillary forces acting as the water recedes in the porous structure, while the binder can act to retain the stress resulting from such forces. Starch produced much higher stresses than latex.

Introduction

The application of a coating layer to a base sheet of paper or board improves its optical and printing properties such as uniformity in appearance, gloss, opacity, ink absorption, and spread. The voids within the porous coating have sufficient capillarity to absorb the solvent or diluent rapidly from ink and hence allow the ink to start to set in the brief intervals between successive ink applications, which are characteristic of a modern printing press.

A coating layer typically consists of (i) *water*, so that the coating can be applied as a particulate suspension; (ii) *pigments*, such as ground (GCC) or precipitated (PCC) calcium carbonates, clays, polymeric pigments (such as polystyrene), titanium dioxide, silica, or talc; and (iii) *binders*, which are needed to provide good cohesion of the porous structure formed by pigments and adhesion of this structure to the substrate.

A mixture of pigment and water is referred to as “slurry”, and a mixture of water, pigment, binder, and any other additives is known as a “coating color”. A commercial coating color has a solid content of between 50 and 70% (w/w). This solid content comprises 80–90% (w/w) of pigment and 10–20% (w/w) of binder. Other compounds, such as dispersants, are used in lower percentages to act as stabilizing agents and to make the components compatible in water suspensions. The particle diameters of the mineral pigments usually range from 0.01 to 10 μm . In this work, a layer between 5 and 10 μm thickness was applied to the substrate with a “draw-down rod”, which had a wire wound around it to apply a known volume of slurry or coating color. The layer then underwent progressive drying.

Binders are usually divided into two types: natural (such as starch or protein) and synthetic [such as styrene–butadiene (SB), acrylic latex, or poly(vinyl

acetate)]. Natural binders often result in coatings that have poor optical qualities, partly because of the way in which the coating shrinks during drying. Synthetic binders suffer less from this problem, and so, although they are more expensive, they are becoming increasingly popular.

If the way in which a coating consolidates during drying can be understood, then the process can be controlled and the optical and printing properties optimized. Groves et al.¹ have reviewed techniques for studying the process experimentally, and other workers have modeled it.^{2–4}

Watanabe and Lepoutre⁵ divided the drying process into three phases, separated by two critical concentrations. The slurry or coating color dries until it reaches the *first critical concentration* (FCC), at which a three-dimensional fluid-filled network is formed and particle motion is greatly restricted. In the second phase, the water–air interfaces recede into the surface pores, forming capillary elements and creating a differential capillary pressure that causes a shrinkage of the network. This continues until the *second critical concentration* (SCC) is reached, at which the structure is rigid and air enters as the liquid retreats. So, it is the structure ranging from FCC to SCC that is important with regard to shrinkage forces; before the FCC, particles are suspended in excess solution with no capillary forces present, and after the SCC, the positions of the particles are locked. Ignorance of this locking effect has often led to incorrect conclusions in the literature, especially concerning so-called migration of particulate material, for example, latex as reviewed by Groves et al.¹

In real paper coating applications, the absorbency of the base sheet is a dominant factor in the absorption of liquid. Superimposed on this is the evaporation of liquid from the exposed surface as the coating is dried. The fibers of natural substrates have a partially plastic behavior and can rearrange during drying. The fluid entering the base sheet in real applications comprises water and dissolved chemicals such as pigment stabilizer, a solution known as “serum”.⁶ To reduce these experimental uncertainties and complexities, the samples

* To whom correspondence should be addressed. Tel.: +44 1752 233020. Fax: +44 1752 233021. E-mail: pmatthews@plymouth.ac.uk.

[†] University of Plymouth.

[‡] Omya AG.

in this study were coated onto an impermeable synthetic substrate, which had elastic but not plastic behavior. The weight loss on drying was therefore through evaporation of water from the surface only.

We report a novel indirect method of measuring the forces acting during drying. We observed the extent of curl with respect to the longest dimension of a sample strip, measured with respect to weight loss.⁷ This was converted to a plot of drying stress with respect to percentage weight loss. The porosities of the dry structures were measured by mercury porosimetry, corrected for sample compression. Mechanisms for the drying within the different coating formulations are inferred from the stresses and porosities.

Theory

Each strip of synthetic substrate was assumed to be an elastic bending beam. Standard bending theory was applied, which relates the forces acting on a beam with the actual deflection of the beam itself, as detailed in the appendix. The forces acting on the surface, causing the deformation, could then be calculated if the Young's modulus of the substrate is known. We made four main assumptions: (i) the weight of the substrate was negligible when compared with the forces acting on its surface, (ii) the mechanical properties of the substrate do not change during the drying of the coating layer, (iii) the substrate acts perfectly elastically in the direction of curl, and (iv) the resistance to bending of the drying coating color layer, which is 5–10 μm thick, is negligibly small when compared to that of the 100- μm -thick substrate.

If both the theory and assumptions are correct, then the equations derived in the appendix show that the bending moments should act to curl the samples into shapes following the arcs of circles in the xz plane. The bending did indeed cause such shapes exactly to within the precision of the measurement method.

Clearly, there were structural transitions within the coating itself because it acted as a stress deliverer, and it is these that form the main subject of the investigation.

Materials

Substrate. The synthetic substrate was a synthetic laminate, Synteape⁸ (Arjo Wiggins), made by filling polypropylene with calcium carbonate and stretching it. Its slightly rough surface allowed the coatings to adhere. Its elastic behavior was shown to be anisotropic because of the stretching in one direction during the last stage of its manufacture. It was found necessary to cut the strips parallel to this stretch direction to establish a reproducible elastic behavior. The strips were formed 4.5 cm long (x axis) and 0.5 cm wide (y axis). The thickness of the substrate was 100 μm and its elastic modulus 1.73 GPa.

Pigments. The pigments were based on GCC. This choice of pigment avoided complications such as the anisotropy of clay platelets and the acicularity of aragonitic PCC.⁹ The GCC was a dispersed limestone from Orgon, France, ground to two particle size ranges, named Hydrocarb 60 and Hydrocarb 90 (Omya AG, Oftringen, Switzerland). The samples contained respectively 60% and 90% (w/w) of particles with diameter <2 μm and with a maximum diameter of around 5 μm .

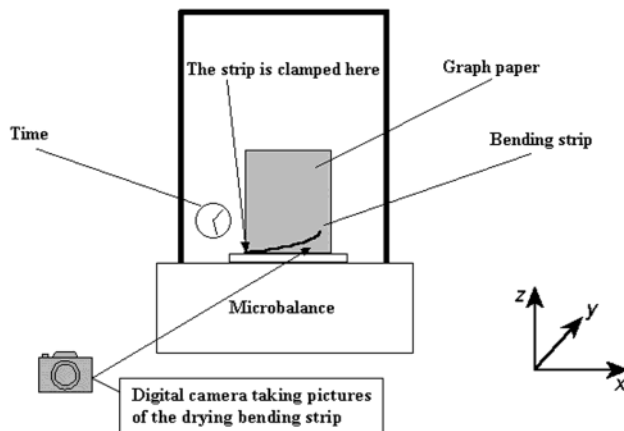


Figure 1. Apparatus.

For a control experiment, the GCC was substituted by a polystyrene pigment with very fine monosize particles, 98% in volume with a diameter less than 0.5 μm (DPP 3710, Dow Chemical, Midland, MI).

Binders. The binder for each sample was selected from one of the following: (i) thermally modified maize starch C-film 07321 (Cerestar, Haubourdin, France); (ii) high glass transition temperature ($T_g = 23$ °C) acrylic latex Acronal S320D in the form of spherical particles of diameter 0.2 μm (BASF, Berlin, Germany); (iii) high- T_g (22 °C) SB latex DL940 (Dow Chemical, Midland, MI) with spherical particles of diameter 0.14 μm ; (iv) low- T_g (5 °C) SB latex DL930 (Dow Chemical, Midland, MI) with spherical particles of diameter 0.15 μm .

Both latex types are designed for stability in the presence of calcium ions, and so the different chemical nature of the acrylic and SB latexes was assumed not to interfere with the study.

The minimum film-forming temperatures are given by the manufacturers as 1 °C above T_g . Therefore, the low- T_g latex was expected to film-form, as much as the coating structure would allow, at the temperature of the experiment (20 ± 1 °C), whereas the high- T_g latexes were not expected to film-form.

Thickness and Composition. The strips were coated using two different draw-down rods: rod 2 (applying about 10 g m^{-2} of dry coating corresponding to a dry coating layer thickness of about 5 μm) and rod 3 (about 20 g m^{-2} and 10 μm , respectively).

Two different compositions were used, either 10% or 25% (w/w) binder on a dry basis, with the remaining being pigment. The 25% (w/w) value is above the maximum binder concentration used in commercial paper coating [typically less than 20% (w/w)] but is included here to demonstrate the independence of the method to critical pigment volume concentration when emulsion polymers are used. Experiments were performed on (i) binders only, (ii) pigment and dispersants only, and (iii) pigment, binders, and dispersants.

Apparatus and Method

The apparatus is shown in Figure 1. The freshly coated strip was clamped at one end and allowed to deform in the vertical xz plane. As deformation progressed, the extent of curl was photographed and the reading on the microbalance noted. Experiments were carried out at 20 ± 1 °C and ambient humidity. It was not necessary to control the humidity because the extent of bending was measured as a function of weight rather than time.

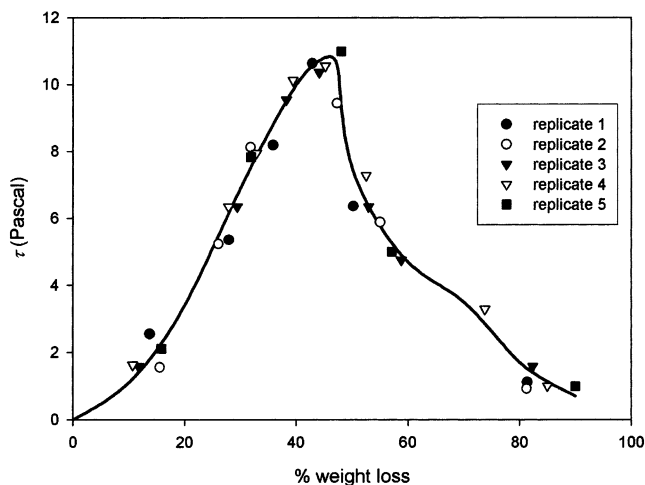


Figure 2. Hydrocarb 90 with 25% high- T_g acrylic latex and low coating weight.

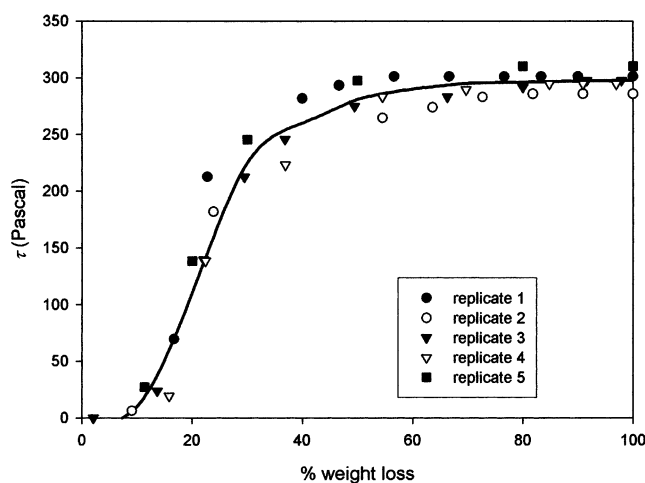


Figure 3. Hydrocarb 90 with 25% starch and low coating weight.

The porosities of the samples were measured by mercury porosimetry. Porosities were corrected for sample compression by applying the equation of Gane et al.,¹⁰ incorporated into the software Pore-Comp:

$$V_{\text{int}} = V_{\text{obs}} - \delta V_{\text{blank}} + \left[0.175(V_{\text{bulk}}^1) \log\left(1 + \frac{P}{1820}\right) \right] - V_{\text{bulk}}^1(1 - \Phi^1) \left\{ 1 - \exp\left[\frac{(P^1 - P)}{M_{\text{ss}}}\right] \right\} \quad (1)$$

where V_{int} is the volume of intrusion into the sample, V_{obs} the intruded mercury volume reading, δV_{blank} the change in the blank run volume reading, V_{bulk}^1 the sample bulk volume at atmospheric pressure, P the applied pressure, Φ^1 the porosity at atmospheric pressure, P^1 the atmospheric pressure, and M_{ss} the bulk modulus of the solid skeletal material.

Results

Stresses. Using the theory described in the appendix, extents of curl were converted to shrinkage force per unit of coated area, i.e., shrinkage stress, τ . Weight losses were expressed as percentage of weight loss relative to the time infinity asymptote. Figures 2 and 3 show the results obtained for five replicates for two different coating formulations. To represent clearly the

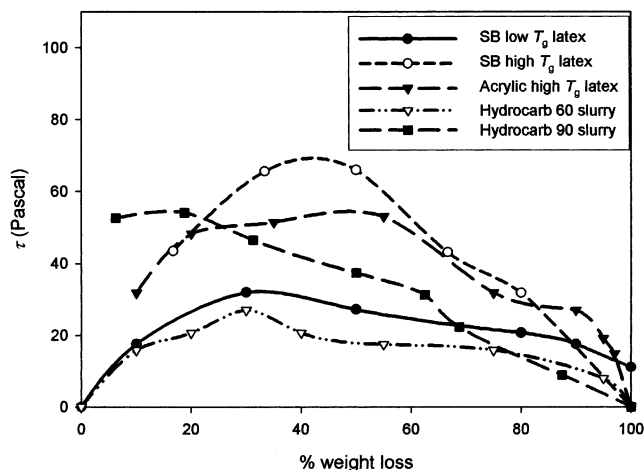


Figure 4. CaCO_3 slurries only; latexes only.

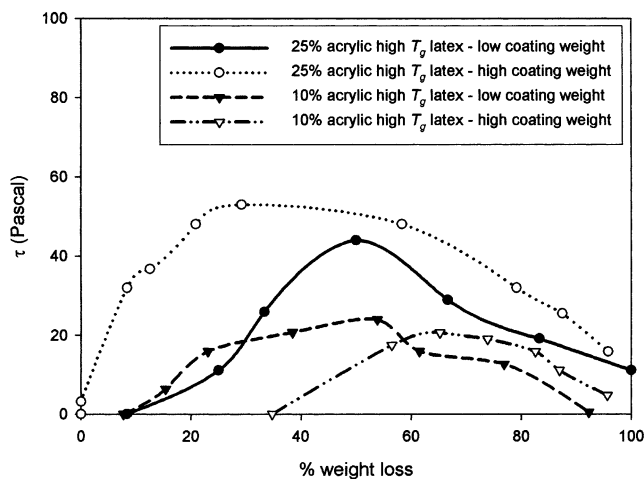


Figure 5. Hydrocarb 60 (coarse) with high- T_g acrylic latex.

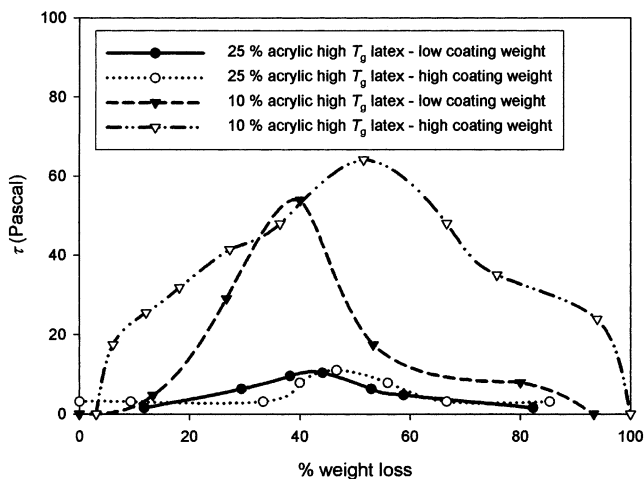


Figure 6. Hydrocarb 90 (fine) with high- T_g acrylic latex.

results for each different coating color formulation, only the results from the replicate closest to the curve fitting the experimental points (replicate 3 in both Figures 2 and 3) were chosen as representative of the behavior of the sample. The average deviations of the experimental points from these curves, relative to the maximum value of the representative curve, were 3.3% and 3.5%, respectively. The same procedure was repeated for each curve shown in Figures 4–13.

First we consider the control experiments containing singly each component of the coating color. The bending

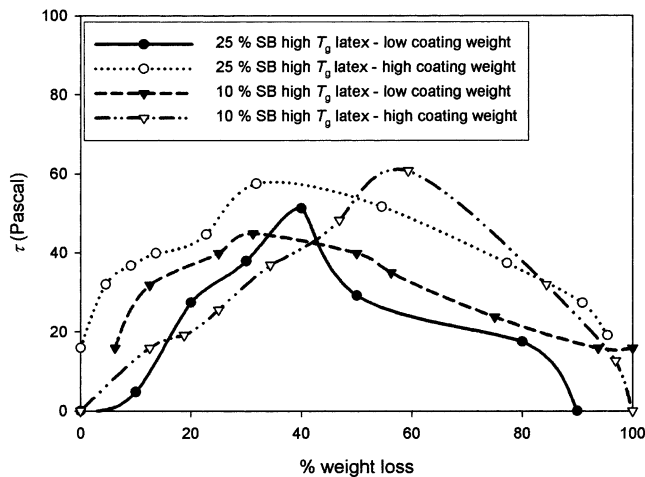


Figure 7. Hydrocarb 60 (coarse) with high- T_g SB latex.

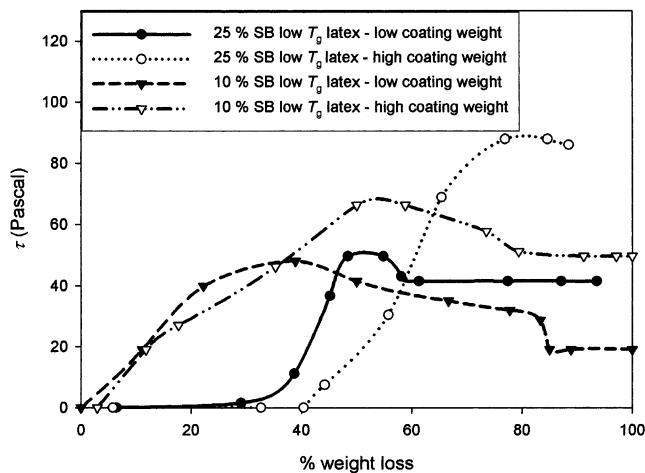


Figure 10. Hydrocarb 90 (fine) with low- T_g SB latex.

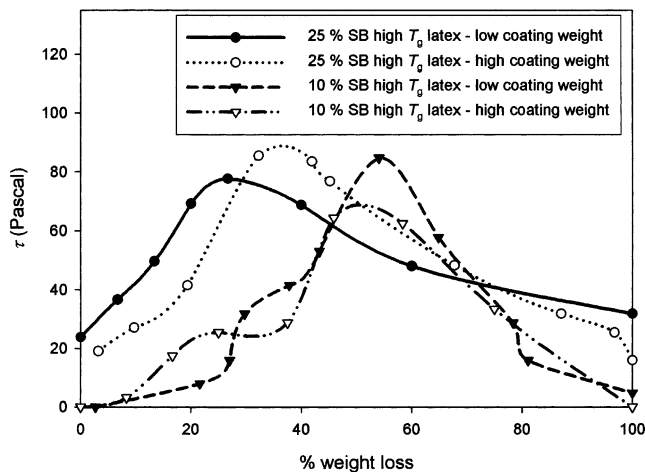


Figure 8. Hydrocarb 90 (fine) with high- T_g SB latex.

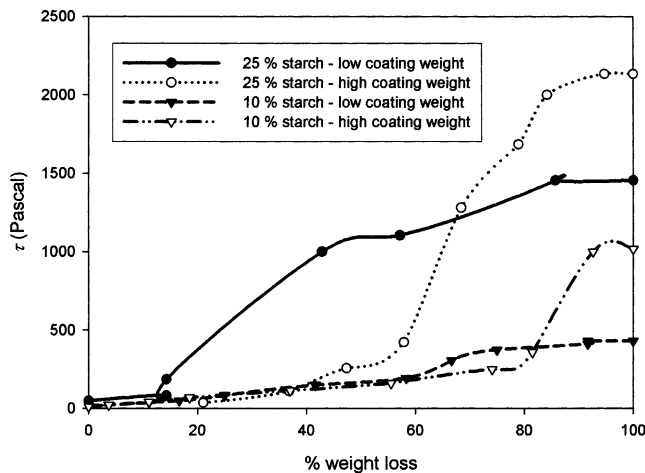


Figure 11. Hydrocarb 60 (coarse) with starch.

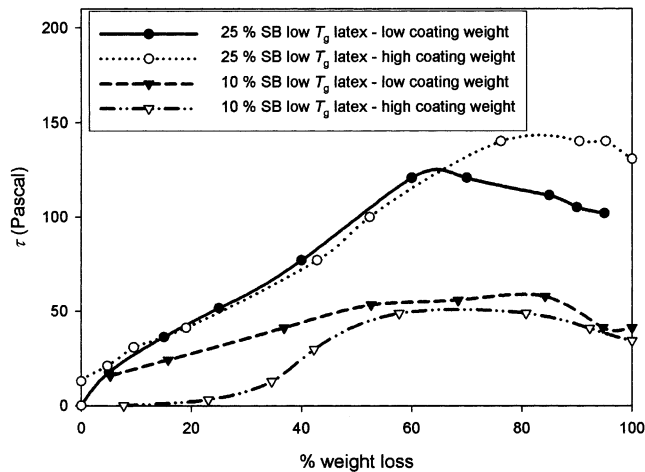


Figure 9. Hydrocarb 60 (coarse) with low- T_g SB latex.

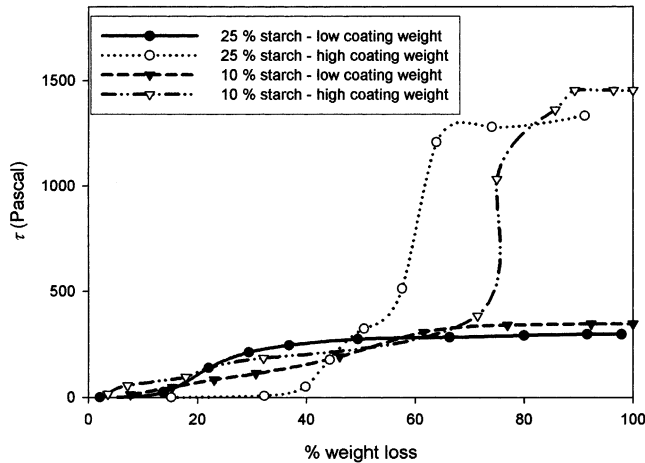


Figure 12. Hydrocarb 90 (fine) with starch.

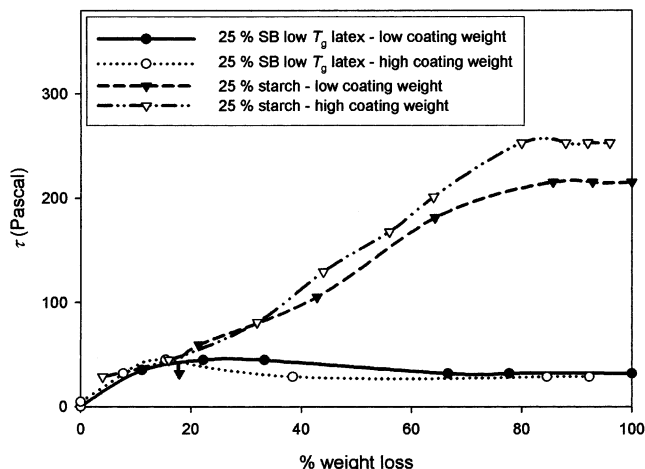
of the samples coated with CaCO_3 slurry or with the latex suspensions alone at low coat weight (using rod 2) was too rapid and too small to be observed with the apparatus. A starch suspension on its own in this experimental setup did not adhere only to the Syntep substrate, but rather it spilled over the sides by edge-wetting capillary forces, fixing the substrate strip to the pan of the microbalance, so that no bending was observed.

Figure 4 shows the results for the CaCO_3 slurries at higher coat weight (rod 3) without binder. The stresses

reached a peak of about 50–60 Pa in the case of the finer mineral pigment (Hydrocarb 90) and 30 Pa in the case of the coarser one (Hydrocarb 60). As the weight loss continued, the stresses in the samples returned to zero. Also shown in Figure 4 are the control experiments with binder suspensions only. The high- T_g latexes gave rise to a maximum stress of about 50–60 Pa and ultimately no stress retention, while the low- T_g latexes showed a smaller stress peak value (30 Pa) and a very small stress retention.

Table 1. Porosities of Dry Samples Measured by Mercury Porosimetry at Indicated Coating Weights

sample	high- T_g acrylic latex		high- T_g SB latex		low- T_g SB latex		starch	
	low	high	low	high	low	high	low	high
HC60 + 10% binder	26.1	24.8	30.8	25.8	21.8	18.7	17.4	15.7
HC60 + 25% binder	19.8	18.9	24.2	19.6	14.2	12.8	14.3	8.0
HC90 + 10% binder	38.4	24.5	39.9	32.2	28.5	24.9	26.5	22.5
HC90 + 25% binder	37.7	23.2	35.1	21.9	15.5	13.9	17.0	10.2
DPP + 25% binder					42.5	33.2	19.3	17.7

**Figure 13.** DPP polystyrene pigment with either low- T_g SB latex or starch.

The graphs in Figures 5 and 6 show the results for complete coating colors. All of the samples contain the high- T_g acrylic latex. It can be seen that the stresses are insensitive to the coat weight and hence the thickness of the coating layer. The amount of latex affected the two different mineral pigments in opposite ways. In the case of the coarser pigment, Figure 5, the maximum stress was around 20 Pa in the case of low binder content and 45–55 Pa in the case of high binder content. For the finer pigment, Figure 6, the maximum stress was very low (11 Pa) for higher binder content and about 50–60 Pa for the lower binder content. In all of these cases, with the high- T_g acrylic latex there was minimal stress retention at the end of the drying process.

Figures 7 and 8 show the results for the pigments together with the high- T_g SB latex. The stresses were relatively insensitive to the thickness of the coating layer and the amount of binder used. There was a small but significant difference between the maximum stress for the coarse calcium carbonate (50–60 Pa), Figure 7, and the fine calcium carbonate (80–90 Pa), Figure 8, as was seen for the CaCO_3 slurries alone. There was once again minimal stress retention for a high- T_g latex.

Figures 9 and 10 show the results for CaCO_3 in the presence of a low- T_g SB latex. The coarser mineral pigment (Figure 9) shows similar trends for similar coating compositions, with the coatings prepared with 25% (w/w) latex showing maximum stresses far larger than those with 10% (w/w). The coating thickness had relatively little effect. Figure 10 shows a mixed behavior: at a low percentage of weight loss, the shrinkage stress is determined by the amount of binder, whereas at higher weight loss, the effect of coating weight becomes more important. The most significant difference is that all of the samples containing the low- T_g SB latex stayed curled indefinitely and retained between 39% and 96% of the maximum stress during drying.

Figures 11 and 12 show the stresses measured on

drying of colors bound with starch. The stresses are an order of magnitude higher than those with latex, and unlike in the cases of slurry only or with latex, those with the coarser calcium carbonate (Figure 11) are higher than those with the finer (Figure 12). The stresses are highly dependent on the coating weight. The amount of starch is seen to affect the coarse pigment samples (Figure 11) but not the fine (Figure 12). All of the samples show a high degree of stress retention, up to 100% of the maximum stress.

As a final control experiment, to test potential interaction phenomena and the effect of the particle size distribution, the broad size distribution calcium carbonate pigments were replaced by the monosized polystyrene pigment DPP 3710, Figure 13, with either 25% (w/w) low- T_g SB latex or 25% (w/w) starch. Unlike the case of starch-containing CaCO_3 -based colors, the thickness of the coating layer did not affect the stress acting upon drying. The maximum stress measured was 230–260 Pa in the case of starch-containing coating colors and 45 Pa, with a stress retention of about 30 Pa on drying, in the case of low- T_g latex-containing coating colors.

Porosities. The porosities of the dry samples, measured as described above, are shown in Table 1.

Discussion

The porosities of the dry samples, Table 1, all decreased upon an increase of the coating weight and layer thickness from rod 2 to rod 3, an effect also observed by other workers.¹¹ The thinner coating layers had a thickness of the same order of size as the largest particles in the layer, and so packing was constrained with respect to the lack of movement of the largest particles. In the thicker coatings, there was a greater possibility of particle movement during drying, and the resulting more efficient packing gave a lower porosity.

Now let us consider the control experiment with the calcium carbonate only, Figure 4. As water evaporates from the structure, menisci recede through it and exert capillary forces. Summed over the whole sample, these forces rise to a stress of nearly 60 Pa between the finer Hydrocarb 90 particles (smaller capillaries and hence high forces) and 30 Pa between the coarser Hydrocarb 60 particles. There is nothing to retain the stress, which, therefore, disappears completely as the sample dries.

Latex on its own produced shrinkage stresses of between 50 and 70 Pa for high- T_g latex and 30 Pa for low- T_g latex. So, menisci forces acted among these arrays of spheres but, as expected, were relieved by the deformability and film-forming tendencies of the low- T_g latex. Starch on its own could not be measured on the current apparatus. However, this is a dissolved binder, and therefore any shrinkage would be due to the shrinkage of the tertiary structures of the polymer chains, a factor not relevant to the mixed polymer carbonate systems that are the focus of this work.

Deducing the processes occurring in the pigment systems with binder is much more difficult because

there is no way of measuring the void structures at the FCC. From the definition of SCC, we can assume that the SCC skeletal structure is the same as that of the dry sample. So, we have to make educated guesses of the FCC structures and match the change from the guessed FCC to the known SCC with the experimental stress and porosity results.

First we compare the Hydrocarb 60 results in Figure 4 (∇) with all of those in Figure 5. It can be seen that the addition of 10% high- T_g acrylic latex reduced the maximum stress from around 30 Pa to around 20 Pa, whereas increasing the amount of latex to 25% increased the maximum stress to between 40 and 50 Pa, dependent on the coating thickness. A possible cause of this is that the binder particles, which are around an order of magnitude smaller than the Hydrocarb 60 particles, create their own secondary porosity. This secondary porosity increases the meniscus forces and hence stresses during shrinkage. However, in doing this, the binder fills gaps within the porous structure. So, increasing the binder concentration from 10% to 25% reduces the porosity from around 25% to around 19%, Table 1.

For the finer Hydrocarb 90, with a low coat weight, there are very high porosities of around 38%, Table 1, but increasing the amount of binder from 10% to 25% has little effect. An explanation is that the Hydrocarb 90 particles are finer and more similar in size to the binder, so that there is no dual-porosity system, as was formerly postulated for the coarser pigment system. The binder and pigment particles pack to give a very open, highly porous structure of 38% or 25% porosity at 10% binder, with stresses similar to those in the Hydrocarb 90 slurry, Figure 4 (\blacksquare), and around 3 times larger than those for Hydrocarb 60 alone. However, unlike Hydrocarb 60, increasing the amount of binder makes the stresses disappear. This suggests that the binder acts to prevent a change in structure between FCC and SCC, although the exact mechanism of this is unclear.

The contribution made by the chemical rather than physical properties of the latex can be inferred by substituting the second high- T_g latex. Comparison of Figures 7 and 8 with Figures 5 and 6 shows that the stress effects are broadly similar, except that the dependence on the amount of binder is now much reduced. Table 1 shows that the porosity effects are also broadly similar for the two types of high- T_g latexes.

Figures 9 and 10 show that the effect of the film-forming low- T_g SB latex is very different. All of the samples now retain the stress when dry. For the coarser Hydrocarb 60, Figure 9, the amount of binder matters but not the coat weight. For the finer Hydrocarb 90, Figure 10, both the amount of binder and the coating weight have an effect. We postulate that the first part of the drying process follows the same mechanism as that for the high- T_g latexes. However, when the FCC has been reached, the latex particles, which are above their minimum film-forming temperature, begin to deform. Being more compressible than the high- T_g latex particles under the forces of capillary action, they allow the deformation of the coating layer (and hence bending of the substrate). The FCC and SCC structures are, therefore, significantly different from each other in both structure and porosity than those for the high- T_g case. Once the structure has reached the SCC, the deformed latex retains a high fraction of the stress. The latex film

occludes much of the pore structure, giving the lower porosities relative to the high- T_g latexes seen in Table 1.

Figures 11 and 12, when compared to the previous graphs, show that the addition of starch increases the stress by more than an order of magnitude relative to the addition of latex. For the coarser Hydrocarb 60, the stress depends on both the coating weight and the amount of added starch, whereas for the finer Hydrocarb 90, Figure 11, only the coating weight is important. An explanation is that partial adsorption of the starch on the pigment particles^{12,13} and/or the relative solubility effect¹⁴ causes a depletion flocculation of the pigment particles, producing an open, loosely packing structure in which groups of flocs touch one another. The lack of close packing reduces the effective number of fine capillary-like voids in the drying coating at the initial FCC. However, once the surface menisci form, the loose floc packing at FCC transforms to the tighter SCC packing as shown by the lower values of dry porosity, Table 1. The change in dimension from loose to tight packing in this system is large, and so the measured stress is correspondingly high.

If a monosized plastic pigment rather than a broad particle size distribution mineral pigment is used, Figure 13, starch produces much lower stresses. This indicates that there is a similarity between FCC and SCC structures when monosized pigments are used and also suggests that with broad size particle distributions there is selective flocculation of different particle sizes of the mineral. With low- T_g SB latexes, the stresses formed in the plastic pigment-containing color are much the same as when CaCO_3 is present, although the structures have even higher porosities, Table 1. All samples retain stress, as expected.

Conclusions

We have presented a novel, indirect method of measuring the stresses in paper coatings that occur as the coating dries.

Latex with a glass transition temperature and film-forming temperature below the temperature of the experiment deformed and retained the stress, manifest in sample strips that remained curled. The results suggested that coarse calcium carbonate particles required a thicker, 10 μm , layer in which to rearrange between the FCC and SCC. Starch produced much higher stresses than latex following flocculation at the FCC. Substitution of the calcium carbonate pigment with a plastic pigment with particles within a narrow size range reduced the stresses.

The results confirm that the shrinkage phenomena affecting the optical and printing properties of coating color formulations prepared using natural binding systems are far larger than those observed for synthetic binding systems. For the first time, the dynamics of such shrinkage phenomena have been observed and quantified.

Despite these useful conclusions and deductions, several questions about the subtle effects of the layer thickness and packing remain unanswered. So, we are in the process of studying the entire mercury intrusion curves rather than just their corrected high-pressure asymptotes, of examining the structures by electron microscopy, of measuring the viscosities of the slurries before application to determine wet-state interactions,

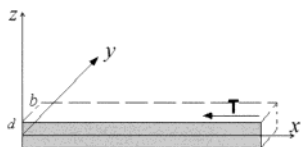


Figure 14. Beam.

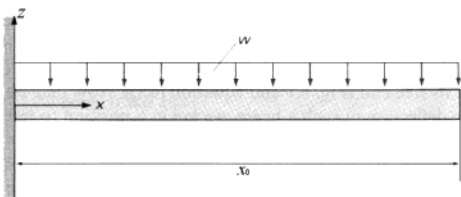
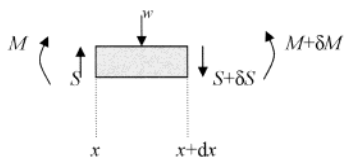
Figure 15. Experiment to measure EI .

Figure 16. Section of a beam.

and of modeling the drying process using a simulated three-dimensional void network.

Appendix¹⁵

Beam Theory. An outline of the elementary beam theory is presented as a guideline for carrying out the full derivation of the working equation for the present experiment.

The elementary beam theory gives

$$M = EI/R \quad (\text{A-1})$$

where M is the bending moment (the torque which develops in a loaded beam as shown in Figure 16), E is the elastic or Young's modulus (the ratio between the stress applied and the subsequent strain), I is the second moment of inertia (a geometrical property of a beam related to its ability to resist bending) related to the z axis (with z as indicated in Figure 14), and R is the radius of curvature of the deformed beam.

Effect of the Coating Layer. It is possible to assume that the coating gives rise to a total surface traction T and, hence, to a bending moment $M = Td$, where $2d$ is the thickness of the beam. From eq A-1

$$EI/R = Td \quad (\text{A-2})$$

where $I = b(2d)^3/12$, b is the width of the beam, and the product EI is called the "beam stiffness".

Radius of Curvature of the Bending Beam. For a generic function $y = f(x)$, the radius of curvature is

$$\frac{1}{R} = \frac{z'}{\sqrt{1 + z'^2}} \quad (\text{A-3})$$

where $z = dz/dx$ and $z' = d^2z/dx^2$. For small z' , $1/R \approx z'$. If we have a circular deformation through (x_0, z_0) , then

$$\frac{1}{R} = \frac{2z_0}{x_0^2 + z_0^2} \quad (\text{A-4})$$

Equations A-3 and A-4 are consistent if $z_0^2 \gg x_0^2$, i.e., for small deformation.

If a deflection z_0 is measured, substituting from eq A-2:

$$Td = \frac{2EIz_0}{x_0^2 + z_0^2} \quad (\text{A-5})$$

If x_0 , z_0 , and EI are known, T can be calculated from eq A-5. The stress acting on the surface of the beam can be calculated as $\tau = T/bx_0$. Because $T \propto I \propto b$, the stress τ is independent of the strip width b .

Evaluation of the Stiffness of the Beam EI . The standard beam theory is also helpful if the stiffness of the beam is unknown. The deflection of the strip is measured because of its own weight, as shown diagrammatically in Figure 15. The effect of the sample weight is assumed to be negligible when compared to the stress caused by the drying coating layer but is nevertheless enough to cause a small deflection. Then it is possible to determine the value of the product EI .

For each section of the beam between x and $x + dx$ (Figure 16), the elementary beam theory gives $dM/dx = S$ and $dS/dx = -w$, where w is the weight per unit of length, M is the bending moment, and S is the shear force.

Setting $1/R \approx z'$ and eliminating S from the previous equations, eq A-1 gives

$$EI \frac{d^4z}{dx^4} = -w \quad (\text{A-6})$$

Successive integrations lead to

$$EIz(x) = -\frac{wx^4}{24} + \frac{wx_0x^3}{6} - \frac{wx_0^2x^2}{4} + Ax + B \quad (\text{A-7})$$

The boundary conditions are

$$z(0) = z'(0) = 0 \quad (\text{A-8})$$

This leads to

$$z(x) = \frac{1}{EI} \left\{ -\frac{w}{24}(x^4 + 6x_0^2x^2 - 4x_0^3x) \right\} \quad (\text{A-9})$$

For $x = x_0$, eq A-9 will become

$$z_1 = z(x_0) = \frac{1}{EI} \left(-\frac{3x_0^4w}{24} \right) = -\frac{x_0^4w}{8EI} \quad (\text{A-10})$$

Finally

$$EI = -\frac{wx_0^4}{8z_1} \quad (\text{A-11})$$

Literature Cited

- (1) Groves, R.; Matthews, G. P.; Heap, J.; McInnes, M. D.; Penon, J. E.; Ridgway, C. J. Binder migration in paper coatings—a new perspective. In *Proceedings of the 12th Fundamental Research Symposium: Science of Papermaking*, Oxford, U.K., 2001; Baker, C. F., Ed.; The Pulp and Paper Fundamental Research Society: Bury, Lancashire, U.K., 2001; ISSN/ISBN 0954112601, pp 1149–1182.
- (2) Pan, S. X.; Davis, H. T.; Scriven, L. E. Modeling moisture distribution and binder migration in drying paper coatings. *Tappi J.* **1995**, *78*, 127–143.

- (3) Bernada, P.; Bruneau, D. Modeling binder migration during drying of a paper coating. *Tappi J.* **1996**, *79*, 130–143.
- (4) Bernada, P.; Bruneau, D. Drying of a paper coating: Experimental Study and Modelling. *Drying Technol.* **1997**, *15*, 2061–2087.
- (5) Watanabe, J.; Lepoutre, P. A Mechanism for the Consolidation of the Structure of Clay-Latex Coatings. *J. Appl. Polym. Sci.* **1982**, *27*, 4207–4219.
- (6) Husband, J. C. Interactions between ground calcium carbonate pigments and polymer latices. *Nord. Pulp Pap. Res. J.* **2000**, *15*, 382–386.
- (7) Perera, D. Y. Stress Phenomena in Organic Coatings. In *Paint and Coating Testing Manual*; Koleske, J. V., Ed.; ASTM manual series; ASTM: West Conshohocken, PA, 1995; pp 585–599.
- (8) Ridgway, C. J.; Gane, P. A. C. Bulk density measurement and coating porosity calculations for coated paper samples. *Nord. Pulp Pap. Res. J.* **2003**, *18*, 24–31.
- (9) Bodurtha, P.; Matthews, G. P.; Kettle, J. P.; Lohmander, S.; James, P. W. The influence of structural anisotropy on fluid permeation in porous media. *2001 Advanced Coating Fundamentals Symposium*, San Diego, CA, 2001; TAPPI Press: Atlanta, GA, 2001.
- (10) Gane, P. A. C.; Kettle, J. P.; Matthews, G. P.; Ridgway, C. J. Void Space Structure of Compressible Polymer Spheres and Consolidated Calcium Carbonate Paper-Coating Formulations. *Ind. Eng. Chem. Res.* **1995**, *35*, 1753–1764.
- (11) Xiang, Y.; Bousfield, D. Effect of Coat Weight and Drying condition on Coating Structure and Ink-Setting. *2001 Advanced Coating Fundamentals*, San Diego, CA, 2001; TAPPI Press: Atlanta, GA, 2001.
- (12) Jarnstrom, L.; Lason, L.; Rigdahl, M.; Eriksson, U. Flocculation in kaolin suspensions induced by modified starches 2. Oxidized and hydrophobically modified oxidized starch in comparison with poly (vinyl alcohol) and carboxymethylcellulose. *Colloids Surf., A* **1995**, *104*, 207–216.
- (13) Jarnstrom, L.; Lason, L.; Rigdahl, M. Flocculation in kaolin suspensions induced by modified starches. 1. Cationically modified starch: effects of temperature and ionic strength. *Colloids Surf., A* **1995**, *104*, 191–205.
- (14) Yan, Y. D.; Burns, J. L.; Jameson, G. J.; Biggs, S. The structure and strength of depletion force induced particle aggregates. *Chem. Eng. J.* **2000**, *80*, 23–30.
- (15) Frenner, R. T. *Mechanics of Solids*; Blackwell Scientific Publications: Malden, MA, 2003; pp 314–388.

Received for review July 21, 2003

Revised manuscript received October 6, 2003

Accepted November 5, 2003

IE0340138